

A PHYSICAL UNDERSTANDING OF HOW REIONIZATION SUPPRESSES ACCRETION ONTO DWARF HALOS

YOOKYUNG NOH¹, MATTHEW MCQUINN^{1,2}*Draft version May 29, 2022*

ABSTRACT

We develop and test with cosmological simulations a physically motivated theory for how the interplay between gravity, pressure, cooling, and self-shielding set the redshift-dependent mass scale at which halos can accrete intergalactic gas. This theory provides a physical explanation for the halo mass scale that can accrete unshocked intergalactic gas, which has been explained with ad hoc criteria tuned to reproduce the results of a few simulations. Furthermore, it provides an intuitive explanation for how this mass scale depends on the reionization redshift, the amplitude of the ionizing background, and the redshift. We show that accretion is inhibited onto more massive halos than had been thought because previous studies had focused on the gas fraction of halos rather than the instantaneous mass that can accrete gas. A halo as massive as $10^{11} M_{\odot}$ cannot accrete intergalactic gas at $z = 0$, even though typically its progenitors were able to accrete gas at higher redshifts. We describe a simple algorithm that can be implemented in semi-analytic models, and we compare this algorithm implemented on top of a halo merger tree to the results in the simulations.

Subject headings: cosmology: theory — large-scale structure of universe — intergalactic medium — galaxies: dwarf — galaxies: formation

1. INTRODUCTION

How gas travels from the intergalactic medium into halos and ultimately onto galaxies is an important input for models of galaxy formation. It is thought that gas accretion is inhibited at halo masses of less than $10^9 - 10^{10} M_{\odot}$, for which thermal pressure from the photoionized intergalactic medium (IGM) suppresses accretion (Shapiro et al. 1994; Quinn et al. 1996; Bullock et al. 2000; Gnedin 2000; Hoeft et al. 2006; Okamoto et al. 2008). This mass scale is set by the complicated interplay between heating, cooling, self-shielding, and gravitational collapse processes.

The halo mass above which intergalactic gas can accrete is a necessary condition on which halos host galaxies, possibly setting the mass scale of the Milky Way's ultra-faint dwarf satellites. A common picture for the formation of these satellites is that they were born prior to reionization, when the lower Jeans' mass of intergalactic gas allowed less massive gas clouds to collapse (Bullock et al. 2000; Gnedin 2000; Somerville 2002; Benson et al. 2002; Busha et al. 2010; Lunnan et al. 2012; Milosavljevic & Bromm 2013). Recent measurements of the stellar ages of the ultra-faint dwarfs, which find advanced ages of ≈ 13 Gyr, have added credence to this simple picture (Brown et al. 2012). A competing theory is that stellar feedback rather than reionization prevents the formation of low mass galaxies (e.g., Dekel & Woo 2003; Mashchenko et al. 2008; Pontzen & Governato 2012). Both reionization and stellar feedback processes play some role in shaping the properties of the smallest galaxies that form in cosmological simulations (e.g., Pawlik & Schaye 2009; Finlator et al. 2011). In addition,

ram pressure stripping by ambient hot gas in the Milky Way halo is a third process that suppresses star formation, at least in satellite galaxies (e.g., Peñarrubia et al. 2008).

In order to disentangle the impact of reionization from other feedback processes, this paper develops a physical understanding for how reionization suppresses galaxy formation. Here 'reionization' refers to the same feedback process that other papers have termed the 'photoionizing background': The heating that pressurized the intergalactic gas occurred predominantly at reionization. Reionization resulted in a pervasive, largely homogeneous hydrogen-ionizing background that maintained intergalactic temperatures of $\sim 10^4$ K and, hence, intergalactic Jeans' masses of $10^9 - 10^{11} M_{\odot}$. We attempt to understand the physics of accretion onto a halo after reionization, as a function of the halo's redshift, the timing of reionization, and the amplitude of the photoionizing background.

Previous analytic and semi-analytic models parametrized the feedback from reionization with simple prescriptions. In particular, many of these models assumed that the Jeans' mass (or similarly the 'filtering mass'; Shapiro et al. 1994; Gnedin & Hui 1998; Gnedin 2000) evaluated at the mean density of the Universe determines the mass scale that is able to accrete (Busha et al. 2010; Lunnan et al. 2012). Unsurprisingly, cosmological simulations show that the Jeans'/filtering mass is *not* a good approximation (Hoeft et al. 2006; Okamoto et al. 2008). Other models have adopted the criterion that gas can accrete onto a halo if its equilibrium temperature (at which photoionization heating balances cooling) evaluated at an overdensity of $60 - 1000$ is greater than the halo virial temperature. While this criterion more successfully reproduces the mass of halos that contain more than half of their baryons (Hoeft et al. 2006; Okamoto et al. 2008), it is

¹ Department of Astronomy, University of California, Berkeley, CA 94720, USA

² Hubble Fellow; mmcquinn@berkeley.edu

unclear physically why it should work.

The impact of reionization on dwarf galaxies has also been studied with 1D codes that follow the collapse of spherically symmetric perturbations (Thoul & Weinberg 1996; Dijkstra et al. 2004; Sobacchi & Mesinger 2013). These 1D investigations quantified how the suppression of gas accretion onto dwarf galaxies depends on a variety of factors, such as the redshift, the thermal history, and the photoionizing background. This paper provides an intuitive picture for many of the trends observed in the 1D calculations. However, the minimum halo mass scale found in the 1D studies is significantly larger at low redshifts than in studies using full 3D cosmological simulations (e.g., Sobacchi & Mesinger 2013). We show that this difference owes to the more gradual buildup of gas by merging that is only captured in the 3D calculations (as hypothesized in Sobacchi & Mesinger 2013).

This paper is organized as follows. Section 2 summarizes the characteristic scales in the problem, using these scales to motivate a simple model for whether a gas cloud is able to collapse. Section 3 describes our cosmological simulations, which are then investigated in the context of our model in Section 4. Finally, Section 5 implements our model in a halo merger tree and compares the results to the simulations. This study assumes a flat Λ CDM cosmological model with $\Omega_m = 0.27$, $\Omega_\Lambda = 0.73$, $h = 0.71$, $\sigma_8 = 0.8$, $n_s = 0.96$, $Y_{\text{He}} = 0.24$, and $\Omega_b = 0.046$, consistent with the favored cosmology by the WMAP CMB experiment plus other large scale structure measurements (Larson et al. 2011).

2. CHARACTERISTIC SCALES

Many of the characteristic scales that factor into whether a halo is able to accrete surrounding gas can be expressed as functions of the temperature and density of ambient gas: (1) the cosmic mean density [and turnaround/virialization densities], (2) the Jeans' mass, (3) the density and temperature at which the cooling time equals the dynamical time, and (4) the density of gas that self-shields to ionizing photons. In what follows, we define these scales and then use them to motivate a physical picture for how gas accretion is inhibited by reionization. This picture is based on the trajectories of gas parcels in the temperature–hydrogen number density (T – n_H) plane, where n_H includes both atomic and ionic species.

2.1. cosmological density scales

The cosmic mean hydrogen number density is

$$\langle n_H \rangle = 1.3 \times 10^{-5} \left(\frac{1+z}{4} \right)^3 \text{ cm}^{-3}, \quad (1)$$

where $\langle \dots \rangle$ indicates a volume average. It is also useful to define the gas overdensity as $\delta_b \equiv n_H / \langle n_H \rangle - 1$. Densities of relevance to our discussion, in addition to the mean ($\delta_b = 0$), are the turnaround density ($\delta_b \approx 4.6$) and the virialization density ($\delta_b \approx 180$). Turnaround – when a region fully decouples from the Hubble flow such that its density starts increasing – occurs at a redshift of $z_{\text{ta}} = 2^{2/3}(z_{\text{coll}} + 1) - 1$, where z_{coll} is the collapse (i.e., virialization) redshift. These characteristic overdensities and redshifts assume the spherical collapse model (Gunn

& Gott 1972) and $\Omega_m(z) = 1$, which applies in the assumed cosmology at redshifts of $z \gtrsim 1$.

2.2. the Jeans' mass

The Jeans' mass – the mass scale that can overcome pressure and collapse gravitationally – is given by (e.g., Binney & Tremaine 1987)

$$M_J = \frac{4\pi}{3} \rho_m \left(\frac{\pi}{k_J} \right)^3, \quad (2)$$

$$= 4 \times 10^9 \left(\frac{T}{10^4 \text{ K}} \right)^{3/2} \left(\frac{n_H}{10^{-3} \text{ cm}^{-3}} \right)^{-1/2} M_\odot, \quad (3)$$

where

$$k_J \equiv c_s^{-1} t_{\text{dyn}}^{-1}, \quad t_{\text{dyn}} \equiv (4\pi G \rho_m)^{-1/2}. \quad (4)$$

Here, ρ_m is the mass density of gas plus dark matter, c_s is the sound speed (evaluated in eqn. 3 for isothermal gas of primordial composition and adiabatic index $\gamma = 5/3$), and t_{dyn} is the dynamical time.

The coefficient of equation (3) is evaluated at $n_H = 10^{-3} \text{ cm}^{-3}$, which is roughly the density where the Jeans' criterion is most relevant in our models for collapse at $3 < z < 6$ (§2.5). Smaller n_H are relevant for halos at lower redshifts. It also assumed $T = 10^4 \text{ K}$, which is likely a good approximation after the reionization of hydrogen. The temperature increased by orders of magnitude at reionization as reionization heated the intergalactic medium (IGM) to $\sim 2 \times 10^4 \text{ K}$ from $\sim 10 - 1000 \text{ K}$ (Miralda-Escudé & Rees 1994; McQuinn 2012). Afterward, the gas in the Hubble flow cools with the expansion of the Universe, but it can only cool to $0.5 - 1 \times 10^4 \text{ K}$ as at these temperatures adiabatic cooling comes into balance with photo-heating (Hui & Gnedin 1997).

While the Jeans' mass is derived by analyzing the growth of modes in a homogeneous medium, it is also the mass of a region that has diameter set by the distance a sound wave travels in a dynamical time. In addition, to factors of order unity it sets when the thermal energy of a cloud equals the gravitational energy (ignoring the kinetic inertia of collapse, which is much smaller unless the cloud is near the virialization density). Thus, even for the case of interest – a collapsing gas cloud – the Jeans' criterion approximates the mass scale at which pressure is able to respond to and halt collapse. Overdense H I absorbers in cosmological hydrodynamic simulations have been found to have sizes of roughly the Jeans' length (Schaye 2001; McQuinn et al. 2011; Altay et al. 2011).

2.3. the equilibrium temperature where atomic cooling balances photoheating

For primordial gas exposed to the extragalactic ionizing background, H I is the dominant coolant at $T \lesssim 5 \times 10^4 \text{ K}$. At higher temperatures, He II cooling can dominate. The dominant heating process for collapsing gas is H I and He I photoionization because the He II in collapsing regions tends to not be exposed to a significant ionizing background (see §2.4). The equilibrium temperature unfortunately cannot be encapsulated with a clean analytic formula. Table 1 gives the equilibrium temperature of primordial gas exposed to a photoionizing background with $\Gamma_{-12} = 1$ and $\Gamma_{-12} = 0.1$, where Γ_{-12}

TABLE 1
THE EQUILIBRIUM TEMPERATURE AT WHICH PHOTOHEATING
BALANCES COOLING,^(*) COMPUTED FOR THE SPECIFIED H I AND
HE I PHOTOIONIZATION RATES AND A HE II PHOTOIONIZATION RATE
OF ZERO.

n_H [cm ⁻³]	$\Gamma_{-12} = 1$	$\Gamma_{-12} = 0.1$
	T_{eq} [10 ⁴ K]	T_{eq} [10 ⁴ K]
1×10^{-5}	41	41
3×10^{-5}	22	22
1×10^{-4}	8.5	8.5
3×10^{-4}	5.9	5.3
1×10^{-3}	3.1	1.9
3×10^{-3}	2.3	1.6
1×10^{-2}	1.8	1.3
3×10^{-2}	1.5	1.2

(*) To the quoted precision, this temperature also equals the temperature at which the cooling time is equal to the dynamical time.

is the H I photoionization rate in units of 10^{-12} s^{-1} . We assume throughout the spectral index of the specific intensity [erg s⁻¹ Hz⁻¹ sr⁻¹] is equal to 0 and that the He I photoionization rate equals that of H I, in accord with ionizing background models (Haardt & Madau 2012). At $2 < z < 5$, observations find $\Gamma_{-12} = 1$ (e.g., Becker & Bolton 2013), with smaller values estimated at lower and higher redshifts (Fan et al. 2006; Haardt & Madau 2012). In addition, we find that the equilibrium temperature is almost identical to the temperature at which the cooling time equals the dynamical time – which is the more applicable criterion. This equivalence results because of the exponential temperature dependence of collisional cooling.

2.4. the density at which gas self-shields

For a gas cloud to self-shield to H I-ionizing photons (such that the optical depth is unity to 1 Ry) requires H I column densities of $N_{\text{HI}} \geq \sigma_{\text{HI}}^{-1} = 1.6 \times 10^{17} \text{ cm}^{-2}$, where σ_{HI} is the H I photoionization cross section at 1 Ry. We denote the fraction of hydrogen that is in H I as x_{HI} , the CASE A recombination coefficient as α , and the electron density as n_e (which equals n_H for ionized gas). If the sizes of intergalactic absorption systems are set by the Jeans' length as previously argued and the gas is in photoionization equilibrium with the background value such that $\Gamma x_{\text{HI}} = \alpha n_e$, then the critical density at which gas self-shields (i.e., has an optical depth of unity at 1 Ry) follows from these relations and is (Schaye 2001)

$$n_H \approx 0.004 \text{ cm}^{-3} \Gamma_{-12}^{2/3} \left(\frac{T}{10^4 \text{ K}} \right)^{0.17}. \quad (5)$$

While equation (5) gives the density that starts to self-shield to an ionizing background, it is not the density that is able to self-shield sufficiently and stay neutral. Studies have found that it requires hydrogen columns of $10 \sigma_{\text{HI}}^{-1}$ to be neutral (Altay et al. 2011; McQuinn et al. 2011, in part because higher energy photons have smaller optical depths), which yields

$$n_H \approx 0.02 \text{ cm}^{-3} \Gamma_{-12}^{2/3} \left(\frac{T}{10^4 \text{ K}} \right)^{0.17}. \quad (6)$$

This number agrees with the radiative transfer calcula-

tions of Faucher-Giguère et al. (2010) with $\Gamma_{-12} \approx 0.5$, which find $n_H \approx 0.01 \text{ cm}^{-3}$ reliably describes the transition to neutral gas.

These self-shielding densities may be important for modeling accretion onto halos for two reasons: First, both atomic cooling and also local sources of radiation become more efficient in self-shielding regions once equation (5) is satisfied.³ Second, collapsing regions that satisfy equation (6) over their entire history are never photoheated. We show in §2.5 that the former has little impact on accretion. We can estimate the redshifts when the latter case occurs in the spherical collapse model: A region is always above this critical density for being fully self-shielded if it collapses at

$$z_{\text{coll}} > 9.3 \left(\frac{\Gamma_{-12}}{0.1} \right)^{2/9} - 1, \quad (7)$$

where we have equated the turnaround density to the density that self-shields as given by equation (6) with $T = 10^4 \text{ K}$. As previously mentioned, $\Gamma_{-12} \approx 0.1$ is consistent with observational estimates at $z \approx 6$ (Fan et al. 2006; Calverley et al. 2011), and the average density is almost certainly smaller with increasing redshift. Thus, galaxies that form from collapse at $z \gtrsim 8$ are typically fully self-shielded and not impacted by photoionization feedback.

He II self-shields more easily than H I. At $z = 2.5$ – when quasars peak in abundance – simple estimates show that the He II self-shields at ~ 30 times lower densities than the H I (McQuinn & Worseck 2013). At lower and higher redshifts, the He II-ionizing background in most regions is expected to be weaker and, hence, the critical density at which self-shielding occurs lower (Worseck et al. 2011). Thus, collapsing regions are likely to be self-shielded to 4 Ry photons once they reach densities where cooling is important, which justifies setting the He II photoionization rate equals zero (as is done subsequently). A more significant He II ionizing background would not alter our picture as it inhibits cooling only in halos collapsing at $z \lesssim 1$ (§2.5).

2.5. gas particle trajectories in the $T - n_H$ plane

The top-left panel in Figure 1 shows where the three characteristic curves described in §2.2–2.4 (as well as curves representing different adiabats) lie in the $T - n_H$ plane:

1. The black dotted diagonal lines represent contours of constant Jeans' mass.
2. The two blue solid curves show where the cooling rate balances the photoheating rate, $T_{\text{eq}}(n_H)$, for the cases $\Gamma_{-12} = 0.1$ (thin) and 1 (thick).
3. The two red (nearly vertical) dashed lines are the thresholds at which gas is fully self-shielded (and hence neutral) for $\Gamma_{-12} = 0.1$ (thin) and 1 (thick). (These curves use the $N_{\text{HI}} = 10 \sigma_{\text{HI}}^{-1}$ criterion for self-shielding. Partial self shielding such that $N_{\text{HI}} = \sigma_{\text{HI}}^{-1}$ occurs at $10^{2/3}$ smaller densities.)

³ One can show that for a typical region, the internal production of ionizing photons can *only* have a significant impact on the photoionization rate in locations that can self-shield (Miralda-Escudé 2005; Rahmati et al. 2013).

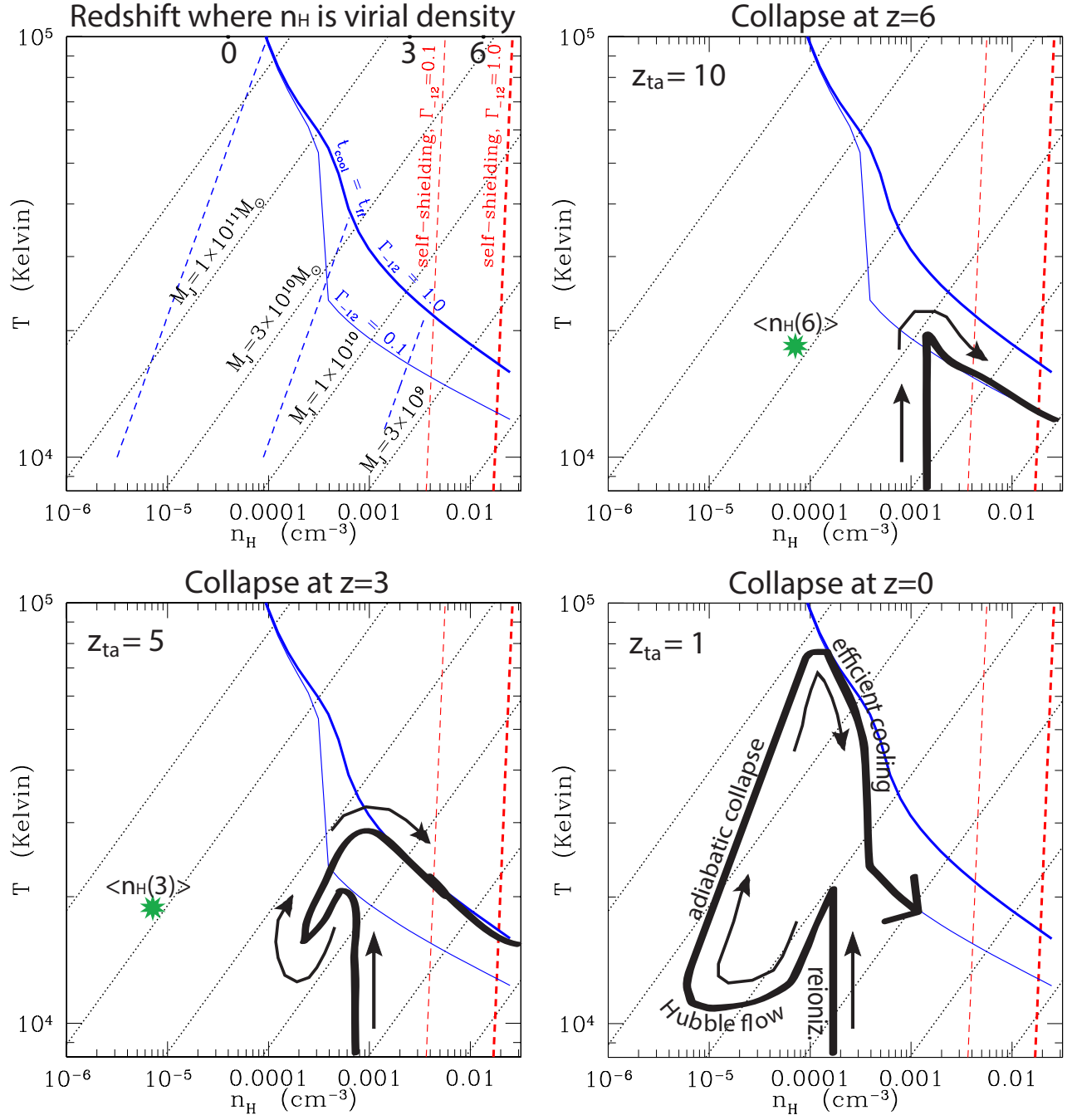


FIG. 1.— Illustration of how gravitationally unstable gas clouds with the specified collapse redshifts travel in the $T - n_H$ plane (assuming no shock heating). The black dotted diagonal lines represent contours of constant Jeans' mass. The blue solid curves show the equilibrium temperature. The nearly vertical, red dashed lines are the thresholds at which gas is fully self-shielded (assuming the $N_{\text{HI}} = 10 \sigma_{\text{HI}}^{-1}$ criterion for self-shielding – partial self shielding occurs at $10^{2/3}$ smaller densities). The two equilibrium temperature curves as well as the two self-shielding curves are computed for $\Gamma_{-12} = 0.1$ (thin) and 1 (thick). In the top-left panel, the three blue dashed diagonal lines that intersect the cooling curves are adiabats (i.e., $T \propto n_H^{2/3}$). The thick black solid curves in the other three panels illustrate schematic trajectories of gas particles accreted onto halos at $z = 6$, $z = 3$, and $z = 0$. The main phases of the trajectory are labeled in the $z = 0$ panel; the $z = 3$ ($z = 6$) trajectory spends less (zero) time in the Hubble flow and adiabatically collapsing. The green stars in the $z = 6$ and $z = 3$ panels are the cosmic mean hydrogen density at the collapse redshift – the density at which many studies had evaluated the Jeans' mass (or filtering mass) to determine the minimum halo mass that can host a galaxy.

4. The blue dashed lines show three example adiabats ($T \propto n_H^{2/3}$).

An expanding or collapsing cloud will approximately travel along an adiabat in the region where (1) its cooling time is longer than the dynamical time (i.e., below the solid black curves) and (2) its temperature is greater than 10^4 K (determined by photoheating being in balance with adiabatic cooling; Hui & Gnedin 1997). Finally, the top axis in the top-left panel shows the virialization density for collapse at $z = 0, 3$, and 6 .

The thick solid curve in each of the other three panels of Figure 1 shows a schematic trajectory for a gravitationally unstable gas cloud that collapses at $z = 6$, $z = 3$, and $z = 0$, assuming that the overdensity follows that expected in the spherical collapse model and that reionization heated the gas to 2×10^4 K at $z = 9$. This is the anticipated temperature if stars reionized the Universe (Miralda-Escudé & Rees 1994; McQuinn 2012). In addition, select curves in the top-left panel appear in the three other panels.

Let us start with the thick solid trajectory shown in the top-right panel in Figure 1 for which $z_{\text{coll}} = 6$. This trajectory's turnaround redshift is approximately its reionization redshift. Thus, at turnaround the gas is heated by reionization to values that are sufficient to cool, radiate away energy, and continue collapsing, thus following the $T_{\text{eq}}(n_H)$ curve to higher densities. If instead the cloud collapses onto a halo at lower redshifts than $z_{\text{coll}} = 6$ (the bottom two panels), it would first cool adiabatically as it expands in the Hubble flow (until it reaches a floor in the temperature at $\approx 10^4$ K when cooling balances photo-heating). At turnaround, it would begin to collapse and heat up adiabatically (unless it were shock heated during this phase, which would cause it to ascend to a higher adiabat). Finally, once a gas parcel collapses to densities at which atomic cooling becomes important, the gas is able to radiate away energy and, hence, follow the blue cooling curves to the right. In Figure 1, the gas parcels that are accreted at $z = 6$ and $z = 0$ follow the $\Gamma_{-12} = 0.1$ cooling curve once cooling becomes important, while the gas that was accreted onto a halo at $z = 3$ follows the $\Gamma_{-12} = 1$ curve. These choices are motivated by observational estimates of Γ_{-12} (Bolton et al. 2005).⁴

In our picture, the trajectories shown in Figure 1 would represent gas collapsing into a dark matter halo whose mass is much greater than the Jeans' masses the trajectory intersects. However, the collapse would halt if (roughly) the mass of the accreting halo is less than the Jeans' mass of the gas at any point along the trajectory (meaning that gravity cannot overcome pressure). Notice that the lower the redshift that the gas is accreted, the larger the halo mass that is required to overcome pressure (i.e., the Jeans' mass, which is constant along the dotted curves, increases moving from the bottom right towards the top left of each panel). Thus, whether a gas parcel can be accreted depends on whether its halo is massive

enough so that it is Jeans' unstable at all densities along its trajectory in the $n_H - T$ plane. We test this simple model in the ensuing sections.

2.6. Previous models

The picture for gas accretion given in §2.5 contrasts with previous models in the literature. Gnedin (2000) argued that the 'filtering mass', M_F , the expanding Universe analog of the Jeans' mass, sets the scale at which gas can accrete at redshift z , when reionization occurred at z_{rei} :

$$M_F(z) = \frac{4\pi}{3} \rho_b \left(\frac{2\pi}{k_J} \right)^3 f(z, z_{\text{rei}})^{3/2}, \quad (8)$$

where

$$f(z, z_{\text{rei}}) = \frac{3}{10} \left[1 + 4 \left(\frac{1+z}{1+z_{\text{rei}}} \right)^{2.5} - 5 \left(\frac{1+z}{1+z_{\text{rei}}} \right)^2 \right].$$

This formula for M_F assumes that the temperature of $\delta_b = 0$ gas after reionization is 10^4 K (Gnedin & Hui 1998), which roughly approximates its evolution in our simulations.

In contrast, Okamoto et al. (2008) argued that only halos for which the equilibrium gas temperature at overdensity δ_* is less than the halo virial temperature can accrete. This criterion is given by

$$M_{\text{acc}}(z, \delta_*) = \frac{1}{GH_0} \left(\frac{2k_B T_{\text{eq}}(\delta_*)}{\mu m_p (1+z)} \right)^{3/2} \left(\frac{\Delta_c(z) \Omega_{m,0}}{2\Omega_m(z)} \right)^{1/2}. \quad (9)$$

where $\Delta_c(z) = 18\pi^2 + 82d - 39d^2$, and $d = \Omega_m(z) - 1 = \Omega_{m,0}(1+z)^3 / (\Omega_{m,0}(1+z)^3 + 1 - \Omega_{m,0}) - 1$. Okamoto et al. (2008) found empirically that M_{acc} with $\delta_* = \delta_{\text{vir}}/3$ approximates the mass scale that can instantaneously accrete gas in their simulations, where δ_{vir} is the halo virial overdensity. Whereas, they find M_{acc} with $\delta_* = 1000$ yields the halo mass scale that retains half of its gas.

Lastly, Hoesft et al. (2006) provided the fit to the mass scale that retains half of the gas:

$$\frac{M_c(z)}{10^{10} h^{-1} M_\odot} = \left(\frac{\tau(z)}{1+z} \right)^{3/2} \left(\frac{\Delta_c(0)}{\Delta_c(z)} \right)^{1/2}, \quad (10)$$

where $\tau(z) = 0.73 \times (1+z)^{0.18} \exp[-(0.25z)^{2.1}]$, motivating it with a similar physical picture to that in Okamoto et al. (2008).

In what follows, we will compare our picture for which halo masses can accrete with M_F , M_{acc} , and M_c .

3. SIMULATIONS

We aim to compare our simple picture for accretion outlined in the previous section with gas accretion in 3D cosmological hydrodynamic simulations. We use the smooth particle hydrodynamics (SPH) code GADGET-3 (Springel et al. 2001), run in a mode where gas particles are turned into stars when $\delta_b > 500$ in order to speed up the computation. All of our simulations are in a $10 h^{-1} \text{Mpc}$ on-a-side periodic box, with either 256^3 or 512^3 gas and an identical number of dark matter particles. These simulations were started at $z = 100$ and

⁴ Gas could become heated at the virial shock to higher temperatures than in our illustrative trajectories, especially if it is collapsing onto a $> 10^{12} M_\odot$ halo (Kereš et al. 2005). However, in all but the most massive halos in the Universe, such shocked gas is able to cool in much less than the age of a system and continue condensing.

initialized with 2nd order Lagrangian perturbation theory applied to a glass particle distribution (Crocce et al. 2006), and all of our simulations are initialized with the same random numbers. In the 512³ simulations, which are primarily for demonstrating convergence, additional random numbers were generated for the modes not in the other simulations. The minimum halo mass studied (linking 32 particles) in the 256³ and 512³ simulations is $2.0 \times 10^8 M_\odot$ and $2.4 \times 10^7 M_\odot$, respectively.⁵

In all of the simulations, snapshots were output on intervals of half of a dynamical time for gas with $\delta_b = 180$, resulting in 45 snapshots between $1 < z < 9$. This frequency of outputs ensures that large changes in the density of $\delta_b \lesssim 180$ gas are unlikely between adjacent snapshots. The simulations were terminated at $z = 1$ as the modes on the box scale are nonlinear at lower redshifts.

The simulations model reionization as an instantaneous process, ionizing the H I and He I at $z = 9$ and boosting the temperature to $1 \times 10^4 \text{K}$. He II reionization (which occurs at $z \sim 3$; McQuinn et al. 2009) is ignored for simplicity. Subsequently, gas particles are kept ionized with photoionization rates for the H I and He I of $\Gamma_{-12} = 1$ in simulation SimG1.⁶ This photoionization rate is consistent with what is measured at $z = 2 - 4$ (e.g., Bolton et al. 2005). Simulation SimG10 has the same reionization redshift but $\Gamma_{-12} = 10$, which makes the hydrogen more ionized and hence suppresses cooling. In addition, all of our simulations ignore self-shielding, except SimG1SS which allows gas particles to self-shield if they are more dense than the density criterion of equation (6) evaluated for $T = 10^4 \text{K}$. All of our calculations that include an ionizing background take it to have a spectral index for the ionizing specific intensity of zero. (The spectral index only mildly impacts the H I and He I photoheating rates.) Our ionizing background model is simpler than in previous studies that used complex ionizing backgrounds a la Haardt & Madau (1996), but it captures the relevant physics (and in a more controlled manner). Our simulations do not include stellar or active galactic nuclei feedback prescriptions.

Lastly, we ran adiabatic simulations for the 256³ and 512³ cases (SimAd and SimAd512). These simulations have neither global heating due to reionization nor cooling. Because the adiabatic simulations have an unheated IGM, we will use the differences between these simulations and the others to isolate the effect of pressure on gas accretion.

4. GAS ACCRETION IN COSMOLOGICAL SIMULATIONS

To test our model with the simulations, we aim to isolate gas particles that would have been accreted onto halos if the Universe had never been heated by reionization. These particles are likely to be the ones that were accreted onto halos in our adiabatic simulation, where the intergalactic gas temperatures are generally very low. Since all of our simulations start with the same initial conditions, we identify initially co-spatial particles in the

TABLE 2
THE GADGET-3 SIMULATION SPECIFICATIONS, INCLUDING THE NUMBER OF GAS PARTICLES, N_g , THE H I AND He I PHOTOIONIZATION RATE, Γ_{-12} , AND THE GAS PARTICLE MASS IN UNITS OF $10^6 M_\odot$, m_{SPH} .

Simulation	BoxSize [Mpc/h]	N_g	Γ_{-12}	m_{SPH}
SimAd	10	256 ³	0	1.1
SimG1	10	256 ³	1	1.1
SimG10	10	256 ³	10	1.1
SimG1SS	10	256 ³	1 ^(*)	1.1
SimAdN512	10	512 ³	0	0.13
SimG1N512	10	512 ³	1	0.13

(*) except with $\Gamma_{-12} = 0$ in self-shielding regions, using equation (6) with $T = 10^4 \text{K}$ for the critical density for self-shielding

other (non-adiabatic) simulations with the particles in the adiabatic simulation. We selected gas particles that are accreted at z_{coll} in the adiabatic simulation, SimAd, with the following three conditions:

1. falls within $1 r_{\text{vir}}$ of each halo's friends-of-friends center of mass,
2. has overdensity above 200 at z_{coll} ,
3. has overdensity below 200 in all of the higher redshifts snapshots ($z > z_{\text{coll}}$).

Following the corresponding gas particles in the simulations that include the heating from reionization and a UV background (i.e., SimG1 and SimG10) will reveal how gas pressure impacts the particles' evolution.

It is illustrative to observe a few example $n_H - T$ trajectories of the selected gas particles. The dotted curves in Figures 2-4 show such trajectories from SimG1 (with the markers indicating the values at the times of simulation outputs), and for reference the solid curve shows T_{eq} . Figures 2, 3, and 4 correspond to $z_{\text{coll}} \approx 1.5, 3$, and 6, respectively. The panels in each figure show the trajectories of four gas particles, which were selected to span a range of halo masses. The legends of these figures specify (1) M_h , the halo mass that the particle would be accreted onto in the absence of pressure, and (2) M_J^{max} . We define M_J^{max} to be the maximum of the Jeans' mass evaluated at any snapshot before the particle crosses the T_{eq} curve. The latter condition avoids including particles with high Jeans' masses that have been heated at the virial shock but still can cool and, hence, are not stabilized by pressure. In the upper panels, particles with $M_h > M_J^{\text{max}}$ are shown, while particles with $M_h < M_J^{\text{max}}$ are shown in the lower panels.

Each simulated SPH particle's trajectory shows a vertical component at the reionization redshift. After reionization, the typical particle evolves to lower densities and temperatures as the universe expands (and in accord with the picture presented in §2.5). If the gas particle is being pulled into a halo with mass M_h that is less massive than M_J at any point during collapse (i.e., $< M_J^{\text{max}}$), pressure is more likely to be able to overcome gravity and prevent collapse. Hence, the particle will continue moving to lower densities in the Hubble flow if it has not reached turnaround before $M_h < M_J$ is satisfied. If it has reached turnaround before this criterion is satisfied,

⁵ We select dark matter halos with GADGET-3's built in Friends-of-Friends halo finder with linking length set to 0.2.

⁶ Many previous studies used J_{21} – the specific intensity in units of $10^{-21} \text{ erg s}^{-1} \text{ Hz}^{-1} \text{ sr}^{-1}$ – instead of Γ_{-12} . $\Gamma_{-12} = 1$ corresponds to $J_{21} = 0.25$ for $\alpha_{\text{bk}} = 0$.

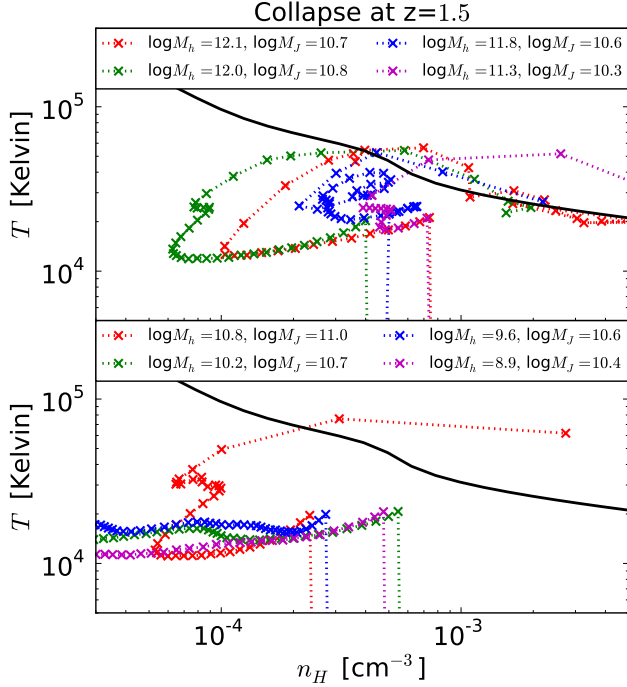


FIG. 2.— The dotted curves in both panels show the trajectories of four gas particles in simulation SimG1. The markers indicate the state of the gas at the times of the simulation outputs. These SPH particles were selected so that their corresponding particle in simulation SimAd crossed the overdensity threshold of $\delta_b > 200$ at $z = 1.5$ and never previously. The vertical component of each trajectory owes to the simulation’s instantaneous reionization at $z = 9$, and the other end of the trajectory corresponds to the state of the gas at $z = 1.5$. The solid curves are the equilibrium temperature at which photoheating balances atomic cooling. The legend lists for each trajectory the halo mass onto which the corresponding particle was accreted in simulation SimAd as well as the trajectory’s maximum Jeans’ mass before crossing the cooling curve, M_J^{\max} . Particles that have $M_h < M_J^{\max}$ are less likely to collapse to high densities, although we find in §4.1 that a more accurate criterion is $M_h < M_J^{\max}/4$.

the trajectory likely will have decoupled from the Hubble flow when it is halted by pressure. Conversely, gas particles that satisfy $M_h > M_J$ over the entire trajectory likely collapse to high densities, radiating their gravitational energy and making it onto a galaxy. However, one can see in Figures 2-4 that while these trends are present, sometimes this criterion errs, especially for particles on the boundary where $M_h \sim M_J^{\max}$. We show later that a better criterion for collapse is $M_h > M_J^{\max}/4$ and even this condition for gravitational stability does not work for every particle.

The model presented in §2.5 assumed that heating from structure formation shocks is not important for determining whether gas can accrete. The trajectories shown in Figures 2-4 validate this assumption. Gas is sometimes heated at a halo’s virial shock as mentioned before, causing it to reach temperatures significantly above the threshold for cooling (e.g., see the red dotted curve in the top panel of Fig. 3). However, such gas cools down in a fraction of the age of the Universe for the $< 10^{12} M_\odot$ halos considered in this study and, hence, does not impact whether the particle reaches high densities. Gas can also shock at densities and temperatures where cooling

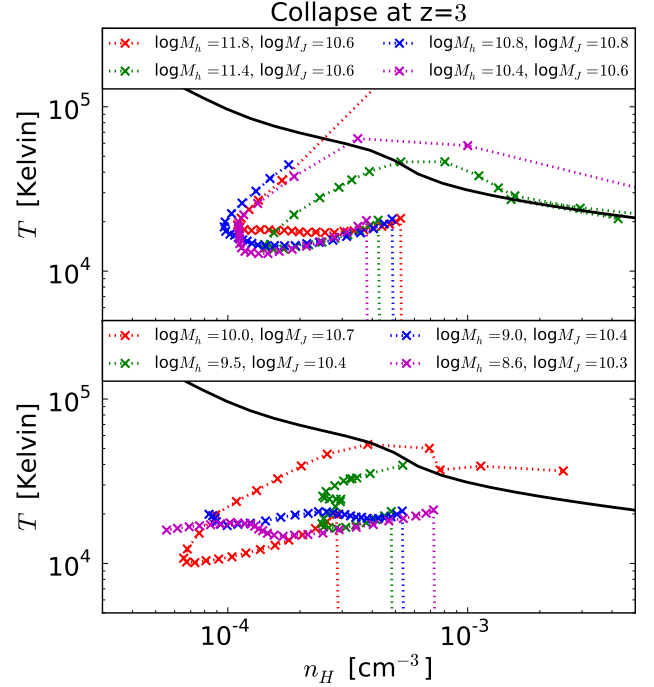


FIG. 3.— The same as Figure 2 except the curves show trajectories of gas particles that would have been accreted at $z = 3$ in the absence of pressure.

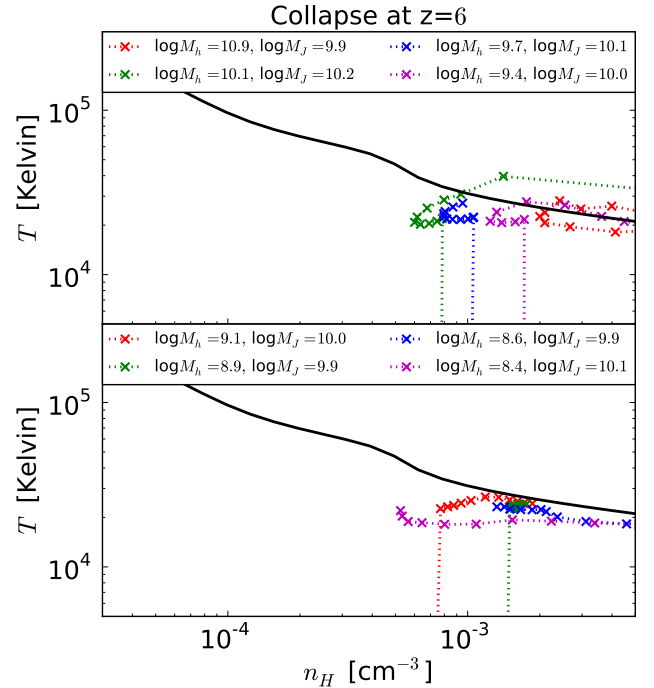


FIG. 4.— The same as Figure 2 except the curves show trajectories of gas particles that would have been accreted at $z = 6$ in the absence of pressure.

is not efficient, and two of the trajectories in Fig. 2 are moderately shock heated during this phase – ascending to higher adiabats. We find that such shocking becomes more probable with decreasing redshift and increasing halo mass. However, a small fraction of the particles we follow show significant shock heating during this phase, justifying our ansatz. Figure 8 discussed in the Appendix shows the trajectories of fifty particles at $z = 1.5, 3$, and 6.⁷

The overall tendency of the SPH particle trajectories shown in Figures 2-4 is consistent with our illustrative plot (Fig. 1). Yet, there are some notable differences. First, the initial gas density varies by a factor of ~ 3 from our spherical collapse predictions. This is because before reionization heats the gas to $\sim 10^4$ K it can clump at much smaller scales than $k_J(T = 10^4 \text{ K})^{-1}$, and it takes a while $[\sim H(z)^{-1}(1 + \delta_J)^{-1/2}]$, where δ_J is the overdensity smoothed at the Jeans’ scale] to thermally relax. It is the larger structures at the scale $\gtrsim k_J(T = 10^4 \text{ K})^{-1}$ that our model considers. Second, most gas particles collapse first into sheets and filaments (or reside in voids swept up by larger collapsing structures) before falling onto halos. This results in turnaround (i.e. decoupling from the Hubble flow) occurring at different densities than in the spherical collapse model. Figure 8 discussed in the Appendix illustrates these trends in more detail.

The characteristics of SPH particle trajectories depend on the redshifts at which they were accreted, as can be noted from comparing Figures 2, 3, and 4. Consider the span of each particle’s trajectory just after its initial vertical rise owing to reionization and before turnaround (i.e., the period it is in the Hubble flow). This span is longer for particles with $z_{\text{coll}} = 1.5$ (Fig. 2) than those with $z_{\text{coll}} = 3$ (Fig. 3). In fact, for some of the particles with $z_{\text{coll}} = 6$, at no time after reionization are they in the Hubble flow (Fig. 4). This is consistent with the qualitative picture presented in §2.5. Second, consider the temperatures that trajectories reach at the time cooling begins to impact their thermal state (i.e., the intersection of the trajectories with the solid curves); the gas reaches higher temperatures for collapse at lower redshifts compared to at higher redshifts (contrast Figures 3 and 4). This tendency again agrees with the picture presented in §2.5. Also, reaching lower densities over the course of a trajectory results in the SPH particle reaching larger Jeans’ masses (noting that the adiabatic phase results in trajectories that are almost parallel to contours of constant Jeans’ mass and so the minimum density is most important for setting M_J ; Fig. 1). Thus, gas needs to sit in larger gravitational potential wells to overcome pressure and be accreted at low redshifts. These trends can be noted by comparing the halo mass to the maximum Jeans’ mass listed in the Figure 2, 3 and 4 keys.⁸

⁷ Our simulations do not include galactic winds. However, our picture shows that such winds would have the largest impact on suppressing accretion if they make it out and shock heat moderate overdensities that characterize the adiabatic collapse phase of the inflows.

⁸ Sometimes a cooling SPH particle follows temperatures and densities that are somewhat (factor of ~ 2) higher than those predicted by the solid T_{eq} curve. This occurs because there is a second stable equilibrium temperature this time below the He II peak (rather than the H I peak) in the cooling rate as a function of density (Field 1965).

We have also investigated how the trajectories depend on the amplitude of the ionizing background and the reionization redshift. We found that the characteristics of trajectories are not substantially altered if we use a 10 times higher ionizing background. In fact, the corresponding trajectories essentially trace each other over much of the path in the simulation with $\Gamma_{-12} = 1$ and $\Gamma_{-12} = 10$ (SimG1 and SimG10): Initially co-spatial particles follow the same path until the particles reach densities at which cooling becomes important, which happens at somewhat higher densities in the case where $\Gamma_{-12} = 10$ than $\Gamma_{-12} = 1$, as our model predicts. Thus, the amplitude of the ionizing background has little impact on the mass scale that can accrete as M_J^{max} is only modestly increased if the SPH particle reaches somewhat higher densities before it can cool efficiently (i.e., the adiabatic and Jeans’ mass contours in Fig. 1 are almost parallel). We also find that when reionization happens has little impact on accretion that occurs well after reionization. In our picture, this results because both gas expanding in the Hubble flow and adiabatically collapsing encounters similar trajectories in $n_H - T$ regardless of the redshift at which reionization happens. We will show that the redshift of reionization is more effective at setting the amount of pre-reionization gas that has accreted onto galaxies.

4.1. calibrating our simple picture

Figures 2-4 illustrate the tendency for a gas parcel that is Jeans’ unstable over all density and temperatures it encounters during collapse to condense to high densities (Fig. 1). This amounts to the criterion that if the mass of the region is larger than M_J^{max} , its gravity overcomes pressure such that gas is able to accrete, whereas if this is not satisfied gas cannot accrete. To test this criterion, we plot M_J^{max} as a function of the halo mass at z_{coll} that they would collapse into in the absence of pressure in Fig. 5, making the ansatz that the halo mass at z_{coll} roughly approximates the “mass of the region”. In Figure 5, each row of panels shows gas particles accreted at $z_{\text{coll}} \approx 6, 3$ and 1.5, from top to bottom. Where possible, the same number of gas particles are shown for each logarithmic halo mass bin. The sampled particles are divided into different panels depending on their densities at z_{coll} . In the lefthand panels, “uncollapsed” particles with $\delta_b < 10$ are shown, whereas the right shows “collapsed” particles with $\delta_b > 200$, with the particle’s color specifying the exact density. Some of the $\delta_b > 200$ particles have become stars and are represented with the dark red color that indicates the color bar’s maximum density.

In Figure 5, the two diagonal dotted lines show $M_h = M_J$ (bottom line) and $M_h = M_J/4$ (top line). The $M_h = M_J/4$ line does a good job at approximating the boundary between gas that cannot accrete onto halos (left panels) and that can (right panels), faring better than the $M_h = M_J$ demarkation. That less massive halos can accrete than given by the criterion $M_h > M_J$ is simple to understand. The Jeans’ length is the distance a sound wave can travel in a dynamical time. However, after turnaround a gas parcel that is collapsing is in free-fall and adiabatically heating up, which means that a sound wave is not able to travel as far as one would predict from the instantaneous density and temperature of a gas particle. Hence, density fluctuations are smoothed

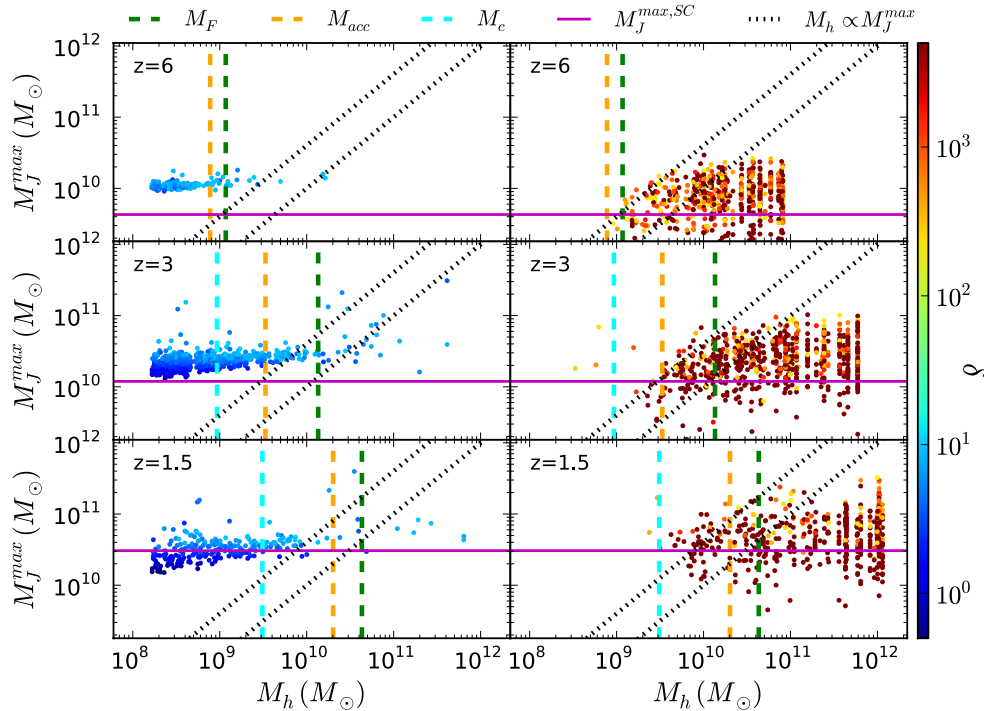


FIG. 5.— The maximum Jeans’ mass of gas particles prior to collapse ($z > z_{\text{coll}}$) in SimG1 as a function of the halo mass that they would be accreted onto in the absence of gas pressure. Each row of panels shows gas particles at $z_{\text{coll}} \approx 6, 3$, and 1.5 , from top to bottom. In each panel, the same number of gas particles are shown for each logarithmic halo mass bin. The sampled particles correspond to those with $\delta_b < 10$ in the left panels and $\delta_b > 200$ in the right. The colors specify the densities, and particles that have turned into stars are given the maximum density on the colorbar. The two diagonal dotted lines are $M_h = M_J^{\text{max}}/4$ and $M_h = M_J^{\text{max}}$ (and the horizontal solid line in each panel shows M_J^{max} if the trajectory follows spherical collapse). For the comparison, the vertical long-dashed lines show the characteristic mass scales reported in previous studies: the ‘characteristic mass’ of Hoefl et al. (2006), the ‘accretion mass’ of Okamoto et al. (2008, evaluating T_{eq} at $\delta_{\text{vir}}/3$), and the ‘filtering mass’ of Gnedin (2000), from left to right respectively.

over a shorter distance than the Jeans’ length, and the effective Jeans’ mass is smaller, as we find. Our finding of a redshift-independent correction factor from the Jeans’ mass criterion is not surprising as the collapse of a spherical perturbation evolves through similar overdensities and temperatures independent of the collapse redshift, at least well after reionization and prior to densities and temperatures are reached at which cooling is efficient.

The proportionality factor of $1/4$ also seems consistent with other indications of the fragmentation mass scale of collapsing cosmological clouds. In 1D collapse calculations, most of the collapse occurs at the collapse redshift and so our instantaneous accretion criterion $M_h \gtrsim M_J^{\text{max}}/4$ should better describe the mass of halos that retain their gas. In fact, the fitting formula for the mass scale that contains half its gas in Sobacchi & Mesinger (2013), $M_{1/2}$, agree well with our prediction of $M_J^{\text{max}}/4$. For collapse at $z = 3$ and $z = 0$ and $\Gamma_{-12} = 1$ Sobacchi & Mesinger (2013) predict $M_{1/2} = 1 \times 10^{10} M_\odot$ and $3 \times 10^{11} M_\odot$, whereas $M_J^{\text{max}}/4$ predicts 1×10^{10} and $1 \times 10^{11} M_\odot$ – the horizontal lines in Fig. 5. These $M_J^{\text{max}}/4$ are calculated assuming spherical collapse and that at turnaround the gas temperature is 10^4 K. In addition, studies of the relation between N_{HI} and δ_b in cosmological simulations find that models based on the

Jeans’ length predict 50% larger densities at fixed N_{HI} (McQuinn et al. 2011; Altay et al. 2011), which indicates that the Jeans’ scale over-predicts the average size of overdense absorbers at a given density by $\sim 50\%$ and, therefore, their mass by a factor of ~ 4 .

As mentioned above, the horizontal line in Figure 5 shows the maximum Jeans mass if the trajectory follows spherical collapse and that $T = 10^4$ K at turnaround. The systematic offset and dispersion around this horizontal line in the *right* panels indicates that for most gas particles collapse is not spherical. Especially with decreasing redshift (where these halos are less rare), the collapse is first into sheets and filaments. In fact, interestingly we find that the average turnaround density, especially at $z = 6$, is somewhat lower than in spherical collapse. The Appendix investigates the spherical collapse approximation in more detail.

Lastly, the long-dashed vertical lines in Figure 5 show the halo mass predicted to contain half of its gas within $1 r_{\text{vir}}$, $M_{1/2}$, in the studies of Hoefl et al. (2006, eqn. 10), Okamoto et al. (2008, eqn. 9) and Gnedin (2000, eqn. 8), from left to right respectively.

5. EXPLAINING THE GAS FRACTION OF HALOS

Most studies of the impact of reionization on galaxies have concentrated on f_{gas} – the gas mass fraction within a virial radius as a function of M_h –, generally fitting for

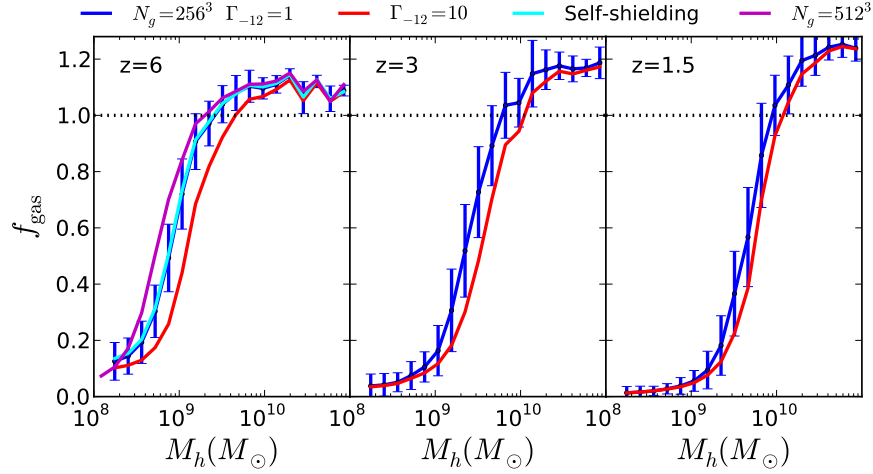


FIG. 6.— Estimated gas fractions within one virial radius, f_{gas} , as a function of halo mass. The curves are computed by taking the ratio of the number of particles within a virial radius in the specified simulation to this number in the adiabatic simulation. This procedure is done individually on each halo and the average is then taken in each halo mass bin. Blue and red solid curves represent the gas fractions in the simulations with $\Gamma_{-12} = 1$ and $\Gamma_{-12} = 10$ (SimG1 and SimG10), respectively. The error bars, shown only for the SimG1 case, give the standard deviation among the halos in each mass bin. The dotted horizontal lines show the maximum, $f_{\text{gas}} = 1$, which the simulation estimates overshoot at the highest masses shown because the halos in the adiabatic simulation are more puffy. The cyan and purple curves in the leftmost, $z = 6$ panel correspond to the simulations with self shielding (SimG1SS) and the 512^3 gas particle simulation that has $8\times$ the resolution of SimG1 (SimG1N512), respectively.

the halo mass that contains half of the baryons, $M_{1/2}$, as a function of redshift (Gnedin 2000; Dijkstra et al. 2004; Hoefft et al. 2006; Sobacchi & Mesinger 2013). Figure 6 shows estimates of f_{gas} in our simulations at $z = 1.5, 3$, and 6 . Our curves overshoot $f_{\text{gas}} = 1$ at high mass because we calculate f_{gas} by dividing the number of gas particles found inside a virial radius in the simulation with cooling with the corresponding number in the adiabatic simulation: The more massive gaseous halos in the adiabatic simulation tend to be puffier and, hence, have fewer particles within r_{vir} . Blue and red solid curves represent the gas fractions in the simulations with $\Gamma_{-12} = 1$ and $\Gamma_{-12} = 10$ (SimG1 and SimG10), respectively. The error bars, shown only for the SimG1 case, give the standard deviation among the halos in each mass bin. The cyan and purple curves in the leftmost, $z = 6$ panel correspond to the simulations with self shielding (SimG1SS) and the simulation with 512^3 gas particles (SimG1N512), respectively. The small differences between these curves and those in the fiducial simulation, SimG1, illustrate that self-shielding has almost no effect and that the convergence in resolution is adequate.⁹ We find that SimG1’s values of $M_{1/2}$ are about a factor of 2 higher than those reported in Okamoto et al. (2008).

These f_{gas} estimates in Figure 6 illustrate the result that there is a relatively well defined halo mass at each

redshift that can accrete gas, with the transition from almost no gas to the cosmic closure density of gas occurring over only a factor of ~ 3 in mass. There is a weak increase in $M_{1/2}$ when increasing Γ_{-12} (compare the blue and red curves which correspond to $\Gamma_{-12} = 1$ and $\Gamma_{-12} = 10$), with the most significant difference occurring in the panel for halos at $z = 6$. This is consistent with our picture in which an increase in Γ_{-12} has a more prominent (but still small) effect at higher redshifts (see Fig. 1).

To test whether our simple prescription for instantaneous accretion explains the simulations’ $f_{\text{gas}}(M_h)$, we implement the prescription described in the previous section into a halo merger tree, using the Neistein & Dekel (2008) merger tree code and assuming spherical collapse. Specifically, we assumed that gas with turnaround redshift after reionization is at a temperature of 10^4 K until its turnaround redshift in spherical collapse, at which time it is heated adiabatically as it collapses. We define $M_J^{\text{max,SC}}(z)$ to be the Jeans’ mass at the point this adiabatic trajectory intersects the equilibrium temperature, where z denotes the collapse redshift. In the merger tree, if $M_h(z) > M_J^{\text{max,SC}}(z)/4$ is satisfied for a halo of mass M_h then that gas can be accreted on it, where $1/4$ is the calibration factor that we found in the previous section. If this criterion is not satisfied for such gas, it is not accreted until a redshift at which the halo has acquired enough dark matter that the criterion is satisfied. At that point, the halo can accrete all of the gas that

⁹ The differences between the 256^3 particle simulation and 512^3 are largest at $z_{\text{coll}} = 6$ compared to the lower redshifts considered in the other panels.

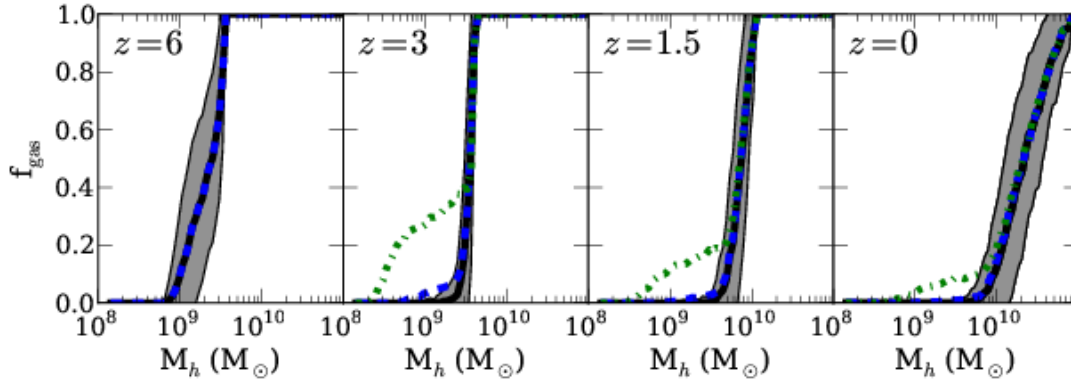


FIG. 7.— The gas mass fraction, $f_{\text{gas}}(M_h, z)$, using the model for accretion discussed in the text implemented on top of a halo merger tree. The black solid curves assume that halos below $3 \times 10^8 M_\odot$ are photoevaporated, and the grey highlighted regions show the standard deviation about the mean value of f_{gas} . The blue dashed curves are the case in which halos with masses below $1 \times 10^8 M_\odot$ are photoevaporated, and the green dot-dashed curve is the same but assume $z_{\text{rei}} = 6$ rather than the fiducial value of $z_{\text{rei}} = 9$. The curves show a similar $M_{1/2}$ compared to the simulations and also have a similar standard deviation in f_{gas} (compare with Fig. 6). However, the transition from zero to one is more abrupt in the merger tree calculations than in the simulations (particularly at $z = 3$).

it had previously been unable to accrete. For gas that has turnaround redshift before reionization but collapse redshift after reionization, we instead apply the criterion for accretion $M_h(z) > M_J(n_{\text{rei}}, T_{\text{eq}}(n_{\text{rei}}))/4$, where n_{rei} is the hydrogen number density of the spherically collapsing parcel at reionization.

The merger tree calculations also must treat halos that formed prior to reionization. Such halos were able to pull in gas down to much lower masses, although many of these halos would also have been photoevaporated prior to merging into larger systems. Barkana & Loeb (2004) found with 1D radiative transfer calculations that $M_h \lesssim 10^8 M_\odot$ halos are photoevaporated by the ionizing background, and they find that this number is reduced only modestly by self-shielding.¹⁰ Our merger tree algorithm leaves the exact mass scale below which halos can be evaporated as a free parameter, which we set to $1 \times 10^8 M_\odot$ and $3 \times 10^8 M_\odot$. The former is closer to what is found in Barkana & Loeb (2004) and the latter to the halo mass “minimally” resolved with 50 particles in our 256³ simulation.

Figure 7 shows the results of this merger tree calculation for $\Gamma_{-12} = 1$ and at four redshifts. The black solid curves take halos with masses below $1 \times 10^8 M_\odot$ to be photoevaporated, whereas the blue dashed curves take $3 \times 10^8 M_\odot$ to be photoevaporated. The differences between these two cases are modest, being largest in the $z = 6$ panel. This figure should be compared to the results from the simulations (Fig. 6). The leftmost three panels in Figure 7 show the same z_{coll} as the three panels in Figure 6. The two figures by-in-large show agreement both in $M_{1/2}$ and the standard deviation in $f_{\text{gas}}(M_h)$. However, especially at intermediate redshifts, the merger tree $f_{\text{gas}}(M_h)$ shows a more abrupt transition from zero to one than $f_{\text{gas}}(M_h)$ in the simulations. This difference likely owes to the merger tree’s simplification of trajec-

ories following spherical collapse and hence having a more uniform M_J^{max} (see the appendix). Still, by $z = 0$ there is a large range of masses in the merger calculations that have $0 < f_{\text{gas}} < 1$.

All of our calculations to this point have taken $z_{\text{rei}} = 9$. In reality, reionization is a complicated process that should span a significant duration in redshift. Some regions may have been reionized as late as $z_{\text{rei}} = 6$, whereas half of the gas was likely ionized at $z > 10$ (Iliev et al. 2006; McQuinn et al. 2007; Trac & Cen 2007; Busha et al. 2010; Lunnan et al. 2012). The dot-dashed green curves in Figure 7 show the results of the merger tree for $z_{\text{rei}} = 6$. In this case, more of a tail develops to low halo masses in the mean f_{gas} . (While not shown, the standard deviation in this dot-dashed curve is comparable to the mean.) The characteristics of this tail (and hence when the local group was reionized) may shape the nature of the Milky Way’s ultra-faint dwarfs. If this is the case, it would also imply the properties of these dwarfs varies throughout the Universe depending on the redshift of reionization (Busha et al. 2010; Iliev et al. 2011; Lunnan et al. 2012).

6. CONCLUSIONS

This paper developed and tested with simulations an intuitive model for how the interplay between gravity, pressure, cooling, and self-shielding set the redshift-dependent mass scale at which halos can accrete gas. This model is based on how the evolution of a collapsing gas cloud is bounded by several critical curves in density–temperature space. This model explains why gas accretion onto halos after reionization is neither strongly impacted by the amplitude of the ionizing background nor the reionization redshift for gas collapsing well after reionization.¹¹

Previous analytic and semi-analytic models assumed that the halo mass threshold above which halos can pull in surrounding gas corresponds to the Jeans’ mass or its

¹⁰ Our self-shielding criterion (eqn. 5) would imply that bound gas within r_{200} of *any* halo would be able to fully self-shield to the ionizing background at $z \gtrsim 8$ for $\Gamma_{-12} = 0.1$ and $T = 10^4$ K. However, this criterion assumes that the scale of fluctuations is the Jeans’ scale for 10^4 K gas, which does not apply to unheated gas or gas that is relaxing after recently being heated (and hence to the photoevaporation of halos).

¹¹ The lack of dependence on Γ_{-12} rules out suggestions that this dependence could regulate star formation and explain why the Universe has what appears to be an extremely-fine tuned, nearly constant ionizing background over $z = 2-5$ (Faucher-Giguère et al. 2008; McQuinn et al. 2011).

cosmological analog, the filtering mass. To determine whether a halo should contain gas, these mass scales had either been evaluated at the mean density of the Universe (Shapiro et al. 1994; Gnedin 2000; Busha et al. 2010; Lunnan et al. 2012) or at densities near the virial density of the halo (Hoeft et al. 2006; Okamoto et al. 2008), leading to a factor of ~ 10 difference in the predicted mass threshold. We showed that neither of these prescriptions is quite right: A spherically collapsing gas parcel encounters densities that are never within an order of magnitude of the cosmic mean density at its z_{coll} . Furthermore, by the time it reaches densities comparable to the virial density of a halo, it will almost certainly continue collapsing and accrete onto a galaxy as it is able to radiate away its energy efficiently. The bottleneck for collapse occurs at densities that are an order of magnitude lower than the virial density and an order of magnitude higher than the cosmic mean density, densities that are not yet able to cool efficiently.

Our model depends on the formation history of a halo rather than its instantaneous halo mass. Capturing the formation history is critical for (1) exploring the hypothesis that the ultra-faint dwarfs formed prior to reionization, and (2) understanding which halos are accreting gas at a given redshift (and hence likely to be forming stars). Regarding (1), our model enabled us to calculate how f_{gas} depends on the local reionization redshift, z_{rei} . While the halo mass at which $f_{\text{gas}}(M_h) = 0.5$ is unaffected by z_{rei} , there is a tail to lower masses of halos that retain $f_{\text{gas}}(M_h) \lesssim 0.2$ that is very sensitive to the local z_{rei} . Regarding (2), by $z = 0$ we found that even a $10^{11} M_{\odot}$ halo is unable to accrete unshocked intergalactic gas, which is a factor of several larger than the mass scale at which $f_{\text{gas}}(M_h) = 0.5$. While not a focus of this paper, our model also illustrates how shock

heating of gas during its “adiabatic” collapse phase (by either structure formation or astrophysical feedback and at temperatures below the equilibrium temperature) can substantially increase the mass threshold that is able to accrete, especially at low redshifts.

A significant drawback of our model is that it lacks a precise analytic criterion for gravitational instability and instead assumes that the masses that are unstable are given by a redshift-independent constant times the maximum Jeans’ mass a gas parcel obtains during collapse. We calibrated this constant with simulations, and gave a physical motivation for the derived value. When this criterion was implemented into a merger tree code that assumed spherical collapse, it was able to reproduce the mass scale at which $f_{\text{gas}}(M_h) = 0.5$, but underestimated the width in M_H of $0.1 < f_{\text{gas}}(M_h) < 0.9$, especially at intermediate redshifts. This underestimate most likely owed to the simplification of spherical collapse; we showed that there is substantial dispersion in what temperatures and densities particles that are accreted at a fixed redshift encounter during their collapse.

This study ignored the impact of outflows from stellar feedback. Outflows may terminate the inflows studied here, preventing them from fueling galaxies. However, even if outflows have a large effect on subsequent accretion, our calculations still determine which halos were able to accrete gas, form stars, and hence later have outflows.

We thank Andrei Mesinger, Robert Feldman, and Nick Gnedin for useful discussions. MM acknowledges support by the National Aeronautics and Space Administration through the Hubble Postdoctoral Fellowship and also from NSF grant AST 1312724.

REFERENCES

- Altay, G., Theuns, T., Schaye, J., Crighton, N. H. M., & Dalla Vecchia, C. 2011, *ApJ*, 737, L37
- Barkana, R., & Loeb, A. 2004, *ApJ*, 609, 474
- Becker, G. D., & Bolton, J. S. 2013, *ArXiv:1307.2259*
- Benson, A. J., Frenk, C. S., Lacey, C. G., Baugh, C. M., & Cole, S. 2002, *MNRAS*, 333, 177
- 1987, *Galactic dynamics*, ed. Binney, J. & Tremaine, S.
- Bolton, J. S., Haehnelt, M. G., Viel, M., & Springel, V. 2005, *MNRAS*, 357, 1178
- Brown, T. M., et al. 2012, *ApJ*, 753, L21
- Bullock, J. S., Kravtsov, A. V., & Weinberg, D. H. 2000, *ApJ*, 539, 517
- Busha, M. T., Alvarez, M. A., Wechsler, R. H., Abel, T., & Strigari, L. E. 2010, *ApJ*, 710, 408
- Calverley, A. P., Becker, G. D., Haehnelt, M. G., & Bolton, J. S. 2011, *MNRAS*, 412, 2543
- Crocce, M., Pueblas, S., & Scoccimarro, R. 2006, *MNRAS*, 373, 369
- Dekel, A., & Woo, J. 2003, *MNRAS*, 344, 1131
- Dijkstra, M., Haiman, Z., Rees, M. J., & Weinberg, D. H. 2004, *ApJ*, 601, 666
- Fan, X., et al. 2006, *AJ*, 132, 117
- Faucher-Giguère, C.-A., Kereš, D., Dijkstra, M., Hernquist, L., & Zaldarriaga, M. 2010, *ApJ*, 725, 633
- Faucher-Giguère, C.-A., Lidz, A., Hernquist, L., & Zaldarriaga, M. 2008, *ApJ*, 688, 85
- Field, G. B. 1965, *ApJ*, 142, 531
- Finlator, K., Davé, R., & Özel, F. 2011, *ApJ*, 743, 169
- Gnedin, N. Y. 2000, *ApJ*, 542, 535
- Gnedin, N. Y., & Hui, L. 1998, *MNRAS*, 296, 44
- Gunn, J. E., & Gott, J. R., III. 1972, *ApJ*, 176, 1
- Haardt, F., & Madau, P. 1996, *ApJ*, 461, 20
- Haardt, F., & Madau, P. 2012, *ApJ*, 746, 125
- Hoeft, M., Yepes, G., Gottlöber, S., & Springel, V. 2006, *MNRAS*, 371, 401
- Hui, L., & Gnedin, N. Y. 1997, *MNRAS*, 292, 27
- Iliev, I. T., Mellema, G., Pen, U., Merz, H., Shapiro, P. R., & Alvarez, M. A. 2006, *MNRAS*, 369, 1625
- Iliev, I. T., Moore, B., Gottlöber, S., Yepes, G., Hoffman, Y., & Mellema, G. 2011, *MNRAS*, 413, 2093
- Kereš, D., Katz, N., Weinberg, D. H., & Davé, R. 2005, *MNRAS*, 363, 2
- Larson, D., et al. 2011, *ApJS*, 192, 16
- Lunnan, R., Vogelsberger, M., Frebel, A., Hernquist, L., Lidz, A., & Boylan-Kolchin, M. 2012, *ApJ*, 746, 109
- Mashchenko, S., Wadsley, J., & Couchman, H. M. P. 2008, *Science*, 319, 174
- McQuinn, M. 2012, *MNRAS*, 426, 1349
- McQuinn, M., Lidz, A., Zahn, O., Dutta, S., Hernquist, L., & Zaldarriaga, M. 2007, *MNRAS*, 377, 1043
- McQuinn, M., Lidz, A., Zaldarriaga, M., Hernquist, L., Hopkins, P. F., Dutta, S., & Faucher-Giguère, C.-A. 2009, *ApJ*, 694, 842
- McQuinn, M., Oh, S., & Faucher-Giguère, C.-A. 2011, *Astrophys.J.*, 743, 82
- McQuinn, M., & Worseck, G. 2013, *ArXiv:1306.4985*
- Milosavljevic, M., & Bromm, V. 2013, *ArXiv e-prints*
- Miralda-Escudé, J. 2005, *ApJ*, 620, L91
- Miralda-Escudé, J., & Rees, M. J. 1994, *MNRAS*, 266, 343
- Neistein, E., & Dekel, A. 2008, *MNRAS*, 383, 615
- Okamoto, T., Gao, L., & Theuns, T. 2008, *MNRAS*, 390, 920
- Pawlik, A. H., & Schaye, J. 2009, *MNRAS*, 396, L46
- Peñarrubia, J., Navarro, J. F., & McConnachie, A. W. 2008, *ApJ*, 673, 226

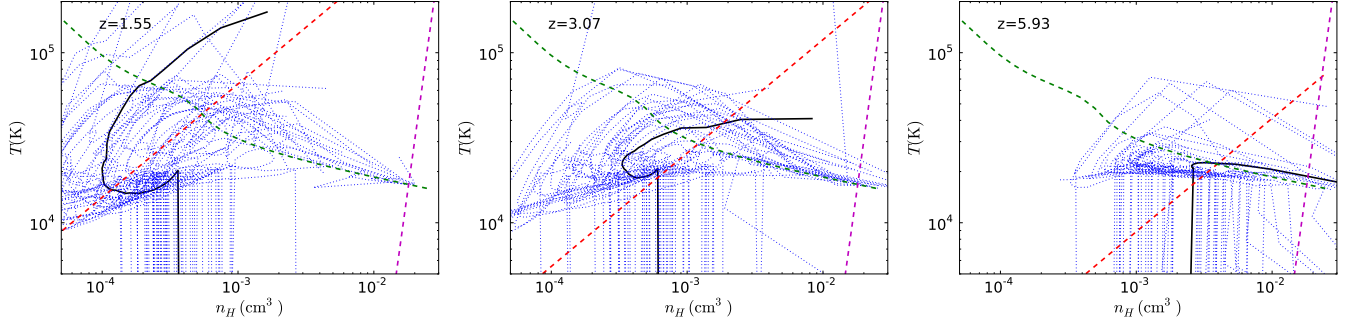


FIG. 8.— The trajectories of particles that collapsed at $z = 1.5$ (left panel), $z = 3$ (middle panel), and $z = 6$ (right panel). The black thick solid curves represent the average trajectory of the particles that crossed the overdensity threshold of $\delta_b > 200$ in SimG1. The blue dotted curves show the trajectories of fifty gas particles randomly selected from among the particles used in the average. The three dashed curves are included for reference and show T_{eq} (green curves), the adiabat for gas at $T = 10^4$ at turnaround in the spherical collapse model ($\delta_{\text{ta}} = 4.6$, red curves), and the self-shielding threshold given by equation 6 (magenta curves). This figure illustrates the approximate nature of the spherical collapse model, which predicts a single $n_H - T$ trajectory if the temperature at turnaround is fixed; the trajectories of the particles that collapse at a single redshift go through a wide range of temperatures and densities.

Pontzen, A., & Governato, F. 2012, MNRAS, 421, 3464
 Quinn, T., Katz, N., & Efstathiou, G. 1996, MNRAS, 278, L49
 Rahmati, A., Schaye, J., Pawlik, A. H., & Raicevic, M. 2013, MNRAS, 431, 2261
 Schaye, J. 2001, ApJ, 559, 507
 Shapiro, P. R., Giroux, M. L., & Babul, A. 1994, ApJ, 427, 25
 Sobacchi, E., & Mesinger, A. 2013, MNRAS, 432, L51
 Somerville, R. S. 2002, ApJ, 572, L23

Springel, V., Yoshida, N., & White, S. D. M. 2001, New Astronomy, 6, 79
 Thoul, A. A., & Weinberg, D. H. 1996, ApJ, 465, 608
 Trac, H., & Cen, R. 2007, ApJ, 671, 1
 Worseck, G., et al. 2011, ApJ, 733, L24

APPENDIX

TRAJECTORIES OF GAS PARTICLES IN $n_H - T$ PLANE

In Figure 8, the black thick solid curves show the average trajectories of SimG1 gas particles selected to have $\delta_b > 200$ at z_{coll} for $z_{\text{coll}} = 6$, 3, and 1.5 (left, middle, and right panel, respectively). The particles used in this average were selected from our subset of gas particles that would have been accreted in SimAd using the accretion criterion described in §4. The average is taken in $\log n_H - \log T$ space. In each figure, fifty trajectories of gas particles (which were randomly selected from among the particles that were used to compute the average trajectory) are shown with the blue dotted lines. In addition, the green dashed curve is the equilibrium temperature at which photoheating balances atomic cooling. The red dashed line is the adiabat along which the gas particles would follow if they collapse at the specified redshift and follow spherical collapse, with $T = 10^4$ at turnaround. The nearly vertical magenta dashed line is the threshold at which gas fully self-shields to hydrogen photoionizations (eqn. 6).

The fifty trajectories show that the gas particles tend to turnaround at somewhat lower density than the turnaround density of $5.6\langle n_H \rangle$ in the spherical collapse model. However, the main trend that is illustrated is that there is broad dispersion in the turnaround redshift. This trend was also apparent in Figure 5 (especially with increasing z), as the M_J^{max} of particles in the simulations was likely to be larger than $M_J^{\text{max,SC}}$ estimated using spherical collapse model. In addition, the average temperature of the trajectories that collapse as z_{coll} tends to lie above T_{eq} at high densities. A higher average temperature than T_{eq} occurs because a larger fraction of gas particles collapsing with decreasing redshift tend to be shock heated at virialization to the virial temperature. This is not surprising because the number of massive halos is larger at lower redshifts.